International Journal of Hydrogen Energy 230 (2026) 154696

Contents lists available at ScienceDirect

International Journal of Hydrogen Energy

journal homepage: www.elsevier.com/locate/he

Advancing sustainable hydrogen production: Urea-assisted alkaline water electrolyzer with circular nickel catalysts

Giulia Alice Volpato [a,b], Andrea Baciami [a,c], Kalina Georgieva Kjurchieva [a], Marco Berton [d,b], Marco Schiavon [d,b], Filippo Bano [a], Alessandra Ferrarini [e], Silvia Galvanin [f], Dario Mosconi [g], Juan Carlos Calderón [c], Silvia Pettenuzzo [a,h], Elena Colusso [b,i,j], Marco Roverso [a], Sara Bogialli [a], Elena Pastor [c], Laura Calvillo [a,j,k], Stefano Agnoli [a,j,k], Mattia Cattelan [a,b,j,k,*]

[a] Department of Chemical Sciences, University of Padova, Via F. Marzolo 1, 35131, Padova, Italy
[b] Centro Studi di Economia e Tecnica dell'Energia Giorgio Levi Cases, Via Gradenigo 6a, 35131, Padova, Italy
[c] Instituto Universitario de Materiales y Nanotecnología, Departamento de Química, Universidad de La Laguna PO Box 456, 38200, La Laguna, Santa Cruz de Tenerife, Spain
[d] Department of Agronomy, Food, Natural Resources, Animals and Environment, University of Padova, Via dell'Università 16, 35020, Legnaro, Padova, Italy
[e] Hyter S.r.l., via Monte Baldo 62, 25015, Desenzano del Garda, Brescia, Italy
[f] Pietro Fiorentini S.p.A., via E. Fermi 8/10, 36057, Arcugnano, Vicenza, Italy
[g] Circular Materials S.r.l., Via Bragni, 93F, 35010, Rettore, Padova, Italy
[h] Department of Civil, Environmental and Architectural Engineering, Università di Padova, via F. Marzolo 9, 35131, Padova, Italy
[i] Department of Industrial Engineering, University of Padova, Via F. Marzolo 9, 35131, Padua, Italy
[j] INSTM Istituto Nazionale Scienza e Tecnologia dei Materiali, Padova Research Unit, Firenze, 50121, Italy
[k] CIRCC Consorzio Interuniversitario per le Reattività Chimiche e la Catalisi, Padova Research Unit, Bari, 70126, Italy

ARTICLE INFO

Keywords:
Sustainable hydrogen
AEMWE
Urea assisted water electrolysis
Circular economy
CFHS nickel
Water-energy nexus

ABSTRACT

In this work, we report a circular-economy approach to hydrogen production through the integration in an anion exchange membrane water electrolyzer (AEMWE) a nickel-based electrocatalyst prepared through circular recovery methods and hybridizing the electrolysis using urea oxidation. $Ni(OH)_2$ and NiO electrocatalysts are recovered from nickel-plating wastewater via a scalable hydrothermal synthesis. Urea, a common environmental pollutant, replaces the oxygen evolution reaction (OER) with urea oxidation, thereby reducing the overall energy demand. Hydrogen production using these circular catalysts and urea achieves performance comparable to benchmark nickel anodes at industrially relevant current densities, with a cell potential reduction of up to 0.25 V relative to OER. Gas chromatography, ion chromatography, and differential electrochemical mass spectrometry (DEMS) analyses identify N_2 and NO_2^- as the main nitrogen-containing products. Carbon adsorption species leads to partial deactivation during prolonged operation; however, the activity can be readily restored by polarity reversal or electrolyte switching. Finally, life cycle assessment (LCA) confirms that coupling urea oxidation with recycled nickel catalysts significantly lowers the CO_2-equivalent footprint of hydrogen production, demonstrating the effectiveness of this circular and energy-efficient approach.

1. Introduction

Hydrogen (H_2) is a key carbon-free energy carrier for decarbonizing the energy sector. Global H_2 output is projected to increase by a factor of 4–8 by 2050, requiring genuinely low-emission production routes [1]. Currently, steam methane reforming dominates supply, accounting for significant CO_2 emissions, whereas "green" H_2 from renewable-powered electrolysis still suffers from the carbon footprint of electricity generation and electrolyzer fabrication [2,3]. Enhancing electrolysis efficiency and adopting sustainable materials is therefore essential for full-chain decarbonization.

The high energy demand of water electrolysis mainly results from the

* Corresponding author. Department of Chemical Sciences, University of Padova, Via F. Marzolo 1, 35131, Padova, Italy.
E-mail address: mattia.cattelan@unipd.it (M. Cattelan).

https://doi.org/10.1016/j.ijhydene.2026.154696
Received 18 December 2025; Received in revised form 27 February 2026; Accepted 22 March 2026
Available online 2 April 2026
0360-3199/© 2026 The Authors. Published by Elsevier Ltd on behalf of Hydrogen Energy Publications LLC. This is an open access article under the CC BY-NC-ND license (http://creativecommons.org/licenses/by-nc-nd/4.0/).

sluggish kinetics of the oxygen evolution reaction (OER), which requires high overpotentials [4]. Precious-metal catalysts such as RuO_X, and IrO_x deliver unmatched activity, particularly in acidic proton exchange membrane (PEM) systems, but their scarcity and cost limit scalability [5]. In alkaline conditions, earth-abundant catalysts (NiO_x, FeO_x, CoO_x) are chemically stable and can approach theoretical overpotential limits [6,7]. This has steered research toward improving alkaline electrolysis as the anion exchange membrane water electrolysis (AEMWE) that merges low-cost electrocatalysts and high current densities of PEM systems. AEMWEs achieve >90 % Faradaic efficiency at <2 V and >1 A cm^{-2} [3,8], with systems demonstrating >10000 h durability at 60 °C and minimal degradation [9,10]. This combination of high performance, low capital cost, and operational robustness positions AEMWE as one of the most promising route for scalable and cost-effective green hydrogen production [3,11].

Following the pursuit of sustainable hydrogen production, research has recently focused on a less demanding anodic reaction, urea oxidation (UOR), which offers the dual benefit of reducing electrolysis energy consumption and valorizing nitrogen-containing waste streams. Urea is produced on an industrial scale (100 Mt yr^{-1}) for fertilizers and chemicals due to its solubility and low toxicity [12], through a relatively energy-efficient process (<6 MJ kg^{-1} of urea) [13], relying on the high temperature-high pressure reaction of ammonia with CO_2, although its overall sustainability is limited by the carbon- and energy-intensive nature of conventional fossil-based ammonia synthesis [14,15]. The development of alternative and sustainable nitrogen sources is thus essential to reduce the environmental impact of urea production. In this context, liquid and sludge livestock effluents, containing substantial amounts of urea (0.5–5 gL^{-1}) and ammonia, emerge as circular nitrogen feedstocks, transforming an environmental burden into a potential resource [12,16,17]. In this study, a 0.33 M urea solution was selected to resemble the concentration typical of mammalian urine [16].

To illustrate the dramatic energy savings of urea assisted electrolysis, consider first classic water splitting at target pH 14 for AEMWE, where the sluggish four-electron oxygen evolution reaction

$$4\ OH^- \rightarrow O_2 + 2H_2O + 4\ e^-\ E^\circ = +0.401\ V \quad \text{eq. 1}$$

paired with the hydrogen evolution reaction

$$2H_2O + 2\ e^- \rightarrow H_2 + 2\ OH^-\ E^\circ = -0.828\ V \quad \text{eq. 2}$$

demands a thermodynamic cell voltage of 1.229 V, which drives high energy consumption [6]. Replacing OER with the UOR

$$CO(NH_2)_2 + 6\ OH^- \rightarrow N_2 + CO_2 + 5H_2O + 6\ e^-\ E^\circ = -0.460\ V \quad \text{eq. 3}$$

reduces the theoretical cell voltage to 0.368 V, corresponding to 70% reduction in driving potential [18].

Interestingly, if we consider urea from livestock's effluents, the produced CO_2 from UOR can be considered biogenic and it can be captured in alkaline media as carbonate,

$$CO_2 + 2\ OH^- \rightarrow CO_3^{2-} + H_2O \quad \text{eq. 4}$$

enhancing carbon neutrality[18].

Conventional three-electrode half-cell electrochemical studies have shown that coupling the UOR with the HER markedly lowers onset potentials, increases current densities, reducing the electricity demand for hydrogen production by roughly 27–30% [19–23] exemplifying a promising strategy for coupling waste treatment with clean energy generation within the water–energy nexus [24].

Despite these synergies, the six-electron UOR mechanism presents significant kinetic barriers that demand advanced catalyst design, particularly involving transition-metal hydroxides and oxides optimized for adsorption/desorption energetics [18,25]. Therefore, the realization of widespread urea-assisted alkaline water electrolysis hinges critically on the development of efficient, durable, and affordable electrocatalysts, and nickel-based materials have emerged as the foremost candidates [23,26–41]. Their earth abundance, low cost, and versatile chemistry enable precising tuning of structural and electronic properties to optimize adsorption and desorption of UOR intermediates. For example, NiOOH/α-FeOOH composites have demonstrated a 90 mV lower overpotential in urea at 50 mA cm^{-2} compared to pure KOH [42], even though the effect of Fe as dopant in Ni-layered double hydroxide (LDH) structure is still discussed and seems detrimental for UOR, rather favoring OER [29]. Mechanistic investigations highlight the formation of active Ni^{3+}-O sites and demonstrate that defect engineering can steer UOR toward N_2 and CO_3^{2-} formation, as seen in Equations (3) and (4), while minimizing side reactions involving nitrogen overoxidation [30,43]. Even though the UOR publications underscore the potential of urea-assisted alkaline electrolysis, there is still the critical need to integrate the UOR into AEMWE systems; however, the effective integration into the state-of-the-art AEMWE technology, as investigated in this work, remains largely unexplored [21,43].

To further reduce the environmental impact of urea-assisted AEMWE technology, we also investigated a sustainable route for electrocatalyst synthesis. A particularly viable route to NiO_x synthesis is based on the recovery from electroless nickel plating (ENP) wastewater via Continuous Flow Hydrothermal Synthesis (CFHS) [44–46]. Recovering Ni via CFHS not only offers a purification strategy for ENP wastewaters, which entail toxicological and ecological hazards [47–53], but also contributes to circular raw material flows, aligning with Europe's Critical Raw Materials Act (CRMA) targets for recycled content [51]. Using CFHS by incorporating modifiers (bases, redox agents, or structure-directing additives) can selectively yield targeted NiO_x phases. Post-synthetic annealing further diversifies the oxide family, all under conditions amenable to scaleup: our industrial scale CFHS reactor produces ≈11 kg day^{-1} of NiO_x, demonstrating industrial viability. CFHS requires only water and electricity, making it one of the "greenest" nanomaterial synthesis methods. Although the most advanced UOR electrocatalysts often rely on multi-element compositions, we chose a single-element system to streamline both synthesis and the supply chain for AEMWE scale-up. While this approach already simplifies sourcing materials, the potential reuse of recycled Ni in other cell components (e.g., gas diffusion layers via sintering) [52], offers an additional route to enhance system circularity, an aspect that will be explored in future work but lies beyond the scope of this study.

In summary, this study tackles two critical challenges in sustainable hydrogen production by integrating a waste-derived NiO_x electrocatalysts, synthesized via CFHS from ENP wastewater, with urea-assisted electrolysis to substantially lower the cell potential required for hydrogen evolution, thus potentially reducing CO_2 emissions and operating costs and improving AEMWE durability. Importantly, we demonstrate these innovations in an actual AEMWE system, one of the few reports of urea-assisted electrolysis under practical operating conditions, alongside lifecycle assessment (LCA) measurements, to deliver realistic insights into energy efficiency, product selectivity, and environmental impact. Together, these strategies exemplify the water–energy nexus, simultaneously producing clean energy, treating waste streams, and providing a clear roadmap for scalable hydrogen technologies. This integrated strategy provides a clear roadmap for scalable, cost-effective, circular electrochemical technologies in the emerging hydrogen economy.

2. Results and discussion

2.1. Structural and morphological analysis

Hereafter we defined as "circular" catalysts the one obtained from CFHS process of ENP sludges [44], see electronic supporting information (ESI) for details. For both the circular nickel catalysts, scanning electron microscopy (SEM) (Fig. S1 and S2) evidenced a peculiar morphology deriving from the ultrafast precipitation induced by the use of supercritical water: small nanoparticles, ranging from less than 5 to 15 nm,

fused or interconnected together forming larger aggregates, in the range 100-500 nm for NiO, indeed it appears as a loose powder, and 100 nm up to 1-2 μm for $Ni(OH)_2$. Despite the thorough washing process, EDX (Table S2 and S3) showed the presence of residual impurities in both the materials, P (3%-10% at. Ratio with respect to Ni, for NiO and $Ni(OH)_2$ respectively) from the synthetic process and a minimal component of iron (up to 6% at. Ratio with respect to Ni) from the initial ENP sludge. This is also confirmed by x-ray photoemission spectroscopy (XPS) analysis, see ESI section 2.2 and Fig. S3, which also confirms the Ni^{2+} oxidation state and the presence of Fe doping, which is especially relevant for NiO [53] and shows that P is not directly linked to the Ni phase but to phosphates [54]. As evidenced from powder XRD (Fig. 1a), circular $Ni(OH)_2$ mainly showed broad peaks corresponding to the β-Ni $(OH)_2$ phase, with the presence of metallic Ni and NiO as a minoritarian component. Conversely, asymmetry of (001) reflection at ca. 19° suggests the presence of stacking faults disorders, which causes selective broadening of preferential directions, a very common fact since β-Ni $(OH)_2$ has a lamellar structure [55]. The XRD of circular NiO revealed also a mixed phase, showing the presence of a metallic nickel component, together with NiO and β-$Ni(OH)_2$. Raman spectra of both catalysts (Fig. 1b) reveal signals consistent with literature for β-$Ni(OH)_2$ in the range of 350-650 cm^{-1}: the lattice mode at 450 cm^{-1} and the acoustic second order lattice mode at around 600 cm^{-1}, which is also present in the spectrum of NiO [56,57]; the weak signals around 1000 cm^{-1} can be ascribed to intercalated anions typical of α-$Ni(OH)_2$, that can be present due to defectivity on *ab*-plane. NiO usually shows distinct bands at 400 cm^{-1} (TO mode) and 530 cm^{-1} (LO mode); however, impurities and small size of circular NiO justify the broadening of the Raman peak [58, 59].

2.2. Electrochemical performance evaluation and UOR selectivity

The intrinsic performance of both catalysts was evaluated by cyclic voltammetries (CVs) in 1 M KOH, with and without the addition of 0.33 M urea (Fig. 2a). The KOH concentration was selected for its industrial relevance in AEMWE systems [3], while the urea concentration was chosen to approximate that found in mammalian urine [16]. For both Ni $(OH)_2$ and NiO, the CVs acquired in absence of urea (darker traces in Fig. 2a) show the typical redox peaks associated with the formation of $Ni^{III}OOH$ during forward (anodic) scan, and reduction of $Ni^{III}OOH$ to $Ni^{II}(OH)_2$ during reverse (cathodic) scan, in agreement with the fact that NiO is known to convert its surfaces in hydroxides after exposure to oxidative potential in alkaline environment [31,60]. Despite having a similar anodic peak potential, $Ni(OH)_2$ exhibits a larger peak separation due to the lower potential of the cathodic peak, which can be attributed to the presence of the more stable β-NiOOH phase, as it is more difficult to reduce.

Electrochemical active surface area (ECSA) was then estimated from the $Ni^{3+/2+}$ reduction peak (Fig. S4 and Fig. 2a), based on the following equation:

$$ECSA\ \left(cm^2\ mg^{-1}\right) = \frac{Q}{0.275 \cdot m} \quad \text{eq.5}$$

where Q (mC cm^{-2}) is the charge associated to the reduction of NiOOH to $Ni(OH)_2$, obtained by dividing the integrated reduction peak current density (in mA cm^{-2}) for the scan rate (V s^{-1}), 0.275 mC cm^{-2} is the charge associated to the formation of one Ni(II) monolayer in 1 M KOH and m (mg cm^{-2}) is the mass loading of deposited catalyst [28]. The calculated ECSA were 8.4 $m^2\ g^{-1}$ and 7.7 $m^2\ g^{-1}$ for $Ni(OH)_2$ and NiO (Fig. 2b), respectively: the relatively high active surface area is in agreement with the SEM morphology, characterized by small interconnected nanoparticles.

Comparison of the CVs acquired in presence and absence of urea, evidenced the higher catalytic activity of $Ni(OH)_2$ toward the UOR with respect to NiO: indeed, despite showing a 20 mV higher UOR onset with respect to NiO, $Ni(OH)_2$ required 1.60 V to reach a UOR current of 10 mA cm^{-2}, with 35 mV negative shift with respect to OER. On the contrary, NiO displayed a higher OER activity, which could be ascribed both to the smaller aggregates size and to the *in-situ* transformation of the initial NiO and metallic Ni phases, or to the higher Fe concentration (Tables S1, S2, S3 and Fig. S3b). At higher potentials, OER eventually outperformed UOR because the two reactions compete for the same NiOOH active species, with the intrinsically faster OER pathway prevailing over the slower UOR mechanism [29]. It should be noted that both materials show discrete OER activity, likely arising from a doping effect of the Fe impurities, which have been reported to favor OER [31, 41,60,61]. Tafel analysis further confirmed the beneficial effects of UOR, with $Ni(OH)_2$ and NiO respectively showing a Tafel slope of 40 and 49 mV dec^{-1} for the UOR process, as opposed to 79 and 89 mV dec^{-1} under OER (Fig. S4c) [62–68].

The peculiar trend observed for the UOR cyclic voltammograms, with the reverse scan displaying a higher current than the forward scan, is due to the fact that with increasing overpotentials an excess of NiOOH active phase is formed, leading to an increased catalytic activity during the reverse scan: this could be ascribed to a relatively slow UOR kinetics, resulting in the NiOOH formation rate being faster than its consumption by UOR at higher overpotentials.

The potential-dependent UOR/OER selectivity of the electrocatalysts for the gaseous products was determined via in-situ.

DEMS, and the results are shown in Fig. 2c and d, S5 and S6. A sharp 300-350 mV separation can be immediately noticed between the onset potentials of N_2 and O_2 evolution under UOR conditions for $Ni(OH)_2$ and NiO, with the former, notably, showing an earlier N_2 onset at 1.27 V. Regarding the OER on the studied catalysts, it is important to highlight

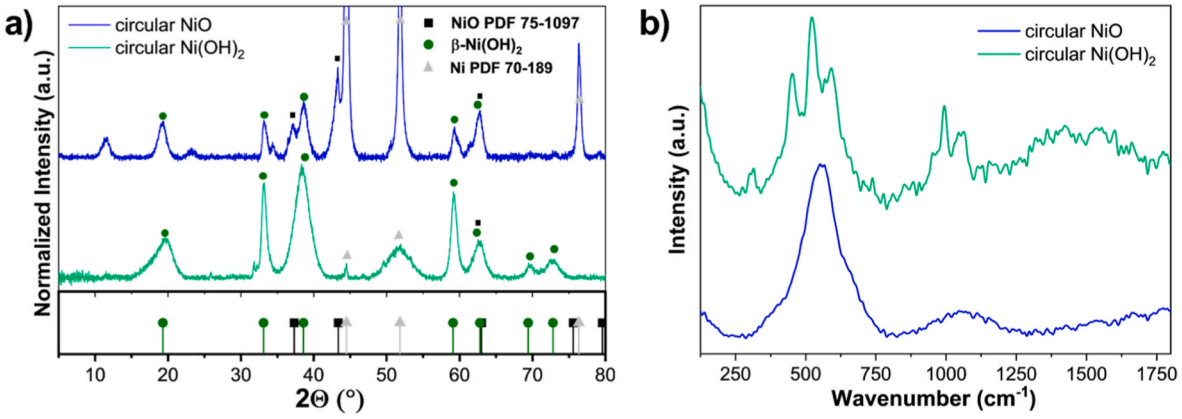

Fig. 1. Physicochemical characterization of circular nickel catalysts, $Ni(OH)_2$ and NiO. (a) Powder X-ray diffraction spectra and corresponding qualitative phase analysis. (b) Raman spectra (λ_{exc} = 532 nm, power = 8 mW).

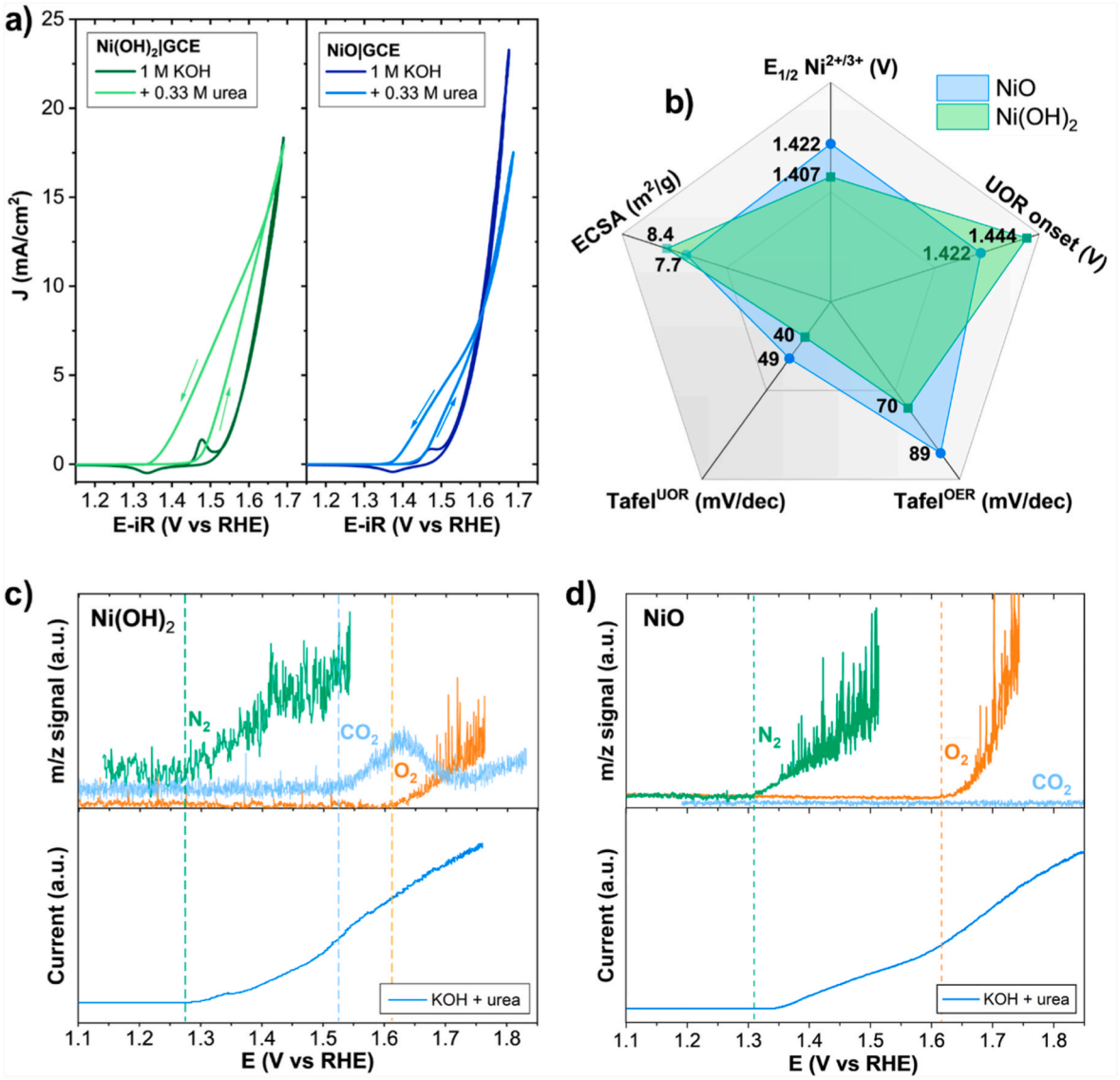

Fig. 2. Half-cell electrochemical characterization of circular nickel catalysts, $Ni(OH)_2$ and NiO. (a) Polarization curves under OER (1 M KOH) and UOR (1 M KOH + 0.33 M urea) conditions for $Ni(OH)_2$ and NiO deposited on glassy carbon electrodes (0.3 mg cm^{-2}). Scan rate: 5 mV s^{-1}; RE: MOE; CE: carbon rod. (b) Radar plot reporting the key Figures of merit extracted from the polarization curves in a. (c, d) In situ detection via DEMS of evolution of N_2 ($m/z = 28$), CO_2 ($m/z = 22$, UOR) and O_2 ($m/z = 32$, OER) (top) during CV scan at 0.5 mV s^{-1} (bottom) in 1 M KOH + 0.33 M urea with (c) $Ni(OH)_2$ and (d) NiO, deposited on carbon cloth.

that the presence of urea induces a shift towards more positive values in the OER onset potential, from 1.40 to 1.62 V vs RHE, which is attributed to adsorbed urea-derived species inhibiting the catalysts' activity toward this reaction (see Fig. S5 and S6).

The onset potential for nitrogen oxides, such as N_2O and NO, nearly matches the values observed for N_2 on both $Ni(OH)_2$ and NiO, indicating nitrogen overoxidation, as shown in Fig. S5 and S6 [27,30,69]. For $Ni(OH)_2$ the CO_2 onset potential is shifted +250 mV toward positive values with respect to N_2, whereas no CO_2 signal was detected on NiO. It must be taken in account that the $m/z = 28$ signal assigned to N_2 can be also assigned to CO, even though the formation of the latter has not been reported before for UOR catalysed by transition metal in alkaline condition [30,70,71]. It can be proposed that formation of NO_X is most prevalent on NiO, whereas $Ni(OH)_2$ can also reach the complete oxidation of carbon species to CO_2. [30,70]. C-containing intermediate species, as cyanate which is formed with NO_2^- in the C–N cleavage pathway [69,70], likely cause inactivation of NiO active sites at high potentials, consistent with the lower UOR activity shown by NiO at high potentials compared with OER (Fig. 2a), as also hinted by a more evident carbon contamination post UOR (Fig. S3c). DEMS analyses therefore demonstrate a nitrogen overoxidation pathway with formation of NO_x and only limited CO_2 formation (observed for $Ni(OH)_2$ only). Moreover, these results evidence a useful potential window where UOR and OER do not overlap. Further analyses of UOR selectivity were performed in the electrolyzer set-up and are reported in the next section.

2.3. Urea-assisted water electrolysis in AEM-electrolyzer

To assess the applicability of the obtained electrocatalysts, an AEMWE was assembled. To minimize voltage losses, commercially available Pt/C cathode and a commercial AEM were employed. We focused only on the anodic side, where we used Ni foam with spray-coated circular nickel catalyst, compared to two Fe-free reference anodes: i) spray-coated pure $Ni(OH)_2$ prepared via the CFHS using a commercial primary nickel precursor called pure $Ni(OH)_2$ [72] and ii) electrodeposited anodes obtained from primary nickel called NiED. It should be noted that the circular anodes only contain Fe from impurities in the ENP wastewater and therefore are not specifically optimized for

the OER. This unavoidably raises the cell voltage required for water electrolysis (WE) but has the advantage that the circular materials are obtained from a straightforward route recovery from Ni sludge. Although NiFe-LDH is the standard OER catalyst in WE systems [40,41], the presence of Fe in the active layer is known to decrease UOR efficiency [29].

As a UOR-specific system optimization (full details in ESI, section S2.5, Figs. S7 and S8), the electrolyzer operated at 50 °C in dual feed mode, with an high anolyte flow of 100 mL min^{-1}: owing to the increased production of gasses during UOR (N_2 and CO_2), an anolyte flux of at least 50 mL min^{-1} was found to be necessary, in our setup, to allow for efficient gas removal, otherwise making UOR less efficient than OER at medium-high current densities. The high temperature both supports reaction kinetics and gas desorption from the electrolyte. The choice of dual feed operation was instead dictated both by the low water permeability of the specific membrane used, limiting cathodic performances in dry cathode, *i.e.* single feed operation, and by the need to maintain OH^- saturation in the membrane, compensating for the formation of carbonates in the anolyte during UOR.

The optimal catalyst loading for spray-coated anodes was found to be in the 1–2 mg cm^{-2}_{geo} range (Fig. 3b and S9), where the subscript *geo* is referred to the geometrical area of the nickel foam substrate. This was ascribed to the balance between nickel foam coverage and catalyst layer thickness, as evidenced from SEM images reported in Fig. S10 and S11: indeed, anodes prepared with higher loadings (3 - 4 mg cm^{-2}_{geo}) showed worse UOR performances, likely due to the thicker catalyst layer (Fig. S9) causing a decrease in pore volume or increased resistance. Anodes were prepared with two different ionomers, proton exchange PFSA and anion exchange Fumion, nonetheless showing similar performances under UOR (Fig. S9).

Under these experimental conditions, a clear potential reduction was observed under UOR at low current densities, with average UOR advantage, defined as the difference between the potentials required for OER and UOR at a given current density, ($\Delta E_{OER\text{-}UOR} = E_{OER} - E_{UOR}$) of 100-200 mV below 0.5 A cm^{-2}, progressively decreasing towards more oxidizing conditions (Fig. 3a and b). However, a few ambiguities emerge

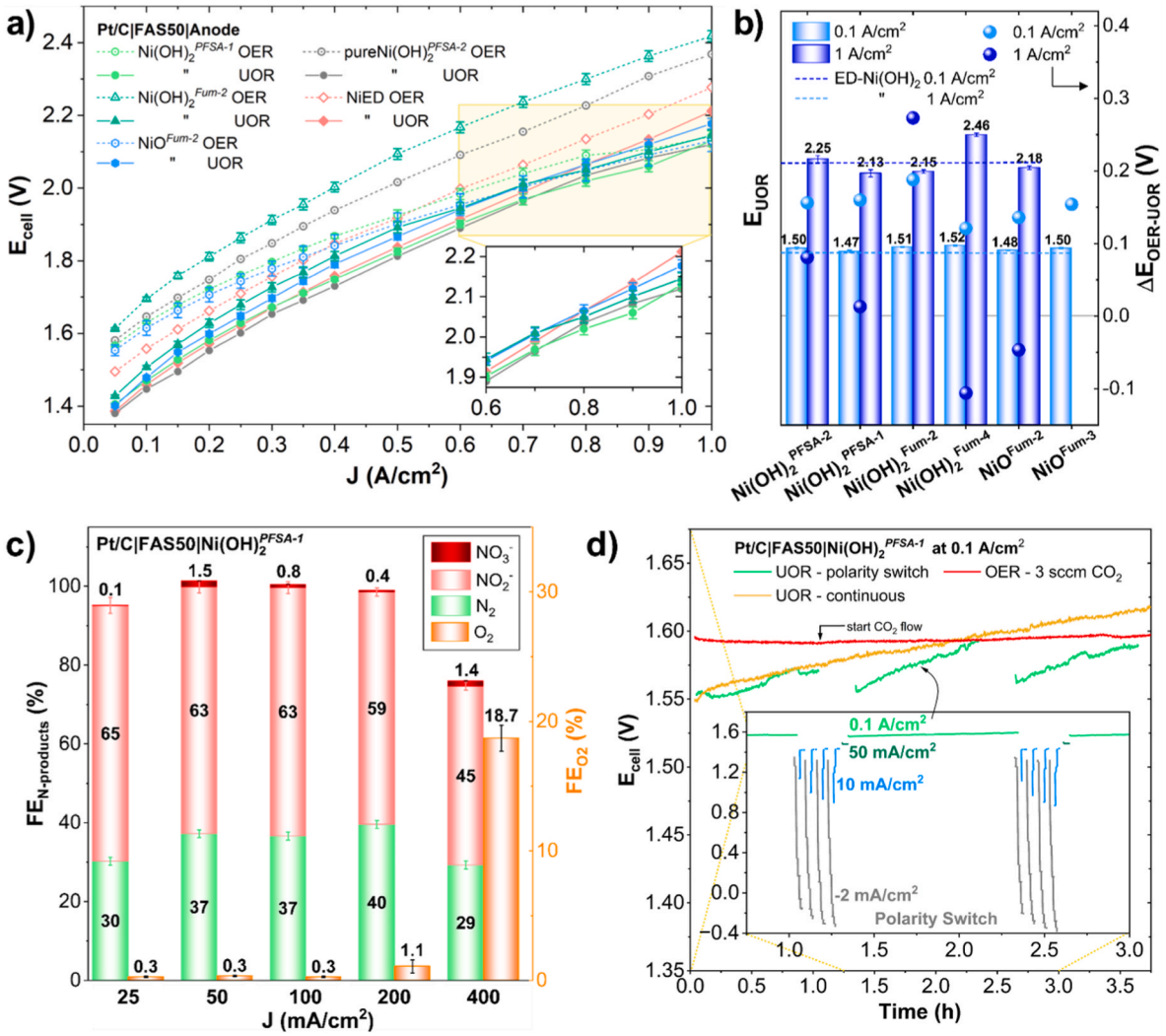

Fig. 3. Electrochemical characterization of urea-assisted water electrolysis on AEM electrolyzer with circular nickel catalysts. (a) Polarization curves in 1 M KOH (OER - dashed line) and 0.33 M urea +1 M KOH (UOR – solid line) for the best performing anodes prepared with circular nickel and different ionomers/loadings, $cat^{ionomer\text{-}loading}$, compared to reference pure $Ni(OH)_2$ (gray) and electrodeposited $Ni(OH)_2$ (NiED – orange) obtained from primary nickel sources. Inset: magnification of the high current region under UOR. (b) Summary of the performances of the tested anodes at 0.1 A cm^{-2} and 1 A cm^{-2} considering UOR potential (left-Y axis - bars) and UOR advantage, $\Delta E_{OER\text{-}UOR} = E_{OER} - E_{UOR}$ (right-Y axis – spheres). (c) Faradaic efficiencies of electrolysis products obtained for increasing current density, performed with $Ni(OH)_2^{PFSA-1}$. (d) Stability tests for $Ni(OH)_2^{PFSA-1}$ under operation at 0.1 A $^{cm-2}$, comparing continuous UOR operation (orange curve) and intermittent UOR operation in 1 M KOH + 0.33 M urea (green curves) with polarity switch (inset, four times switching between −2 mA cm^{-2} and 10 mA cm^{-2} every 2 min). The performance in CO_2-purged 1 M KOH reservoir (OER) is also reported for comparison. (For interpretation of the references to colour in this figure legend, the reader is referred to the Web version of this article.)

when only stating UOR efficiency based on this latter parameter, which intrinsically depends on the OER performance, for example resulting in an apparently higher UOR efficiency for anodes having poorer OER performance: this is the case of $Ni(OH)_2^{Fum-2}$, showing a considerably larger UOR advantage than $Ni(OH)_2^{PFSA-1}$, even reaching 280 mV at 1 A cm^{-2} despite the latter showing both a better OER and UOR performance. In agreement with the results obtained on glassy carbon electrodes, considering anodes with the same loading, NiO showed a lower UOR potential with respect to $Ni(OH)_2$ at $J < 0.7$ A cm^{-2}, though followed by more favorable OER at higher current. This could be either due to further catalyst activation in KOH under strong oxidative conditions, thus favoring OER, or by the poisoning of NiO active sites by adsorbed carbon species [70], as suggested by DEMS analyses. Conversely for $Ni(OH)_2$, UOR remained more favorable than OER even at high J, though with a progressive contraction of the UOR advantage.

Based on these considerations, we identified $Ni(OH)_2^{PFSA-1}$ as the best-performing anode, showing UOR potentials of 1.40 V at 0.05 A cm^{-2}, 1.47 V at 0.1 A cm^{-2} and 2.13 V at 1 A cm^{-2}. Indeed, when compared to NiED, it remarkably showed a similar UOR onset and superior UOR performance at $J > 0.3$ A cm^{-2}, reaching an 80 mV difference at 1 A cm^{-2}. However, it should be noted that, while the UOR advantage of NiED seems unaffected at more oxidizing potentials, a progressive reduction is observed for $Ni(OH)_2^{PFSA-1}$. Pure $Ni(OH)_2$ showed a similar UOR performance to NiED and $Ni(OH)_2^{PFSA-1}$, with slightly improved performance at low current densities where the UOR contribution is more relevant, and it reached an overall greater UOR advantage due to a worse OER performance, with a 0.25 mV difference at 1 A cm^{-2}. Nonetheless, at $J > 0.7$ mA cm^{-2} the UOR performance of $Ni(OH)_2^{PFSA-1}$ is superior or comparable, which is ascribed to the presence of residual Fe impurities, providing a performance advantage by enhancing competing OER at higher current densities.

Therefore, to determine the predominant reaction pathways in different operating regions, products detection was performed at 5 current densities (25, 50, 100, 200, 400 mA cm^{-2}) by means of inline GC for quantification of gaseous products (N_2 and CO_2 from UOR and O_2 from OER) and by ion exchange chromatography coupled to a conductivity detector (IC-CD) on the anolyte for the quantification of nitrite, NO_2^-, and nitrate, NO_3^-, occurring from the overoxidation pathway [27,30]. The measurements were performed with 50 standard cubic centimeters per minute (sccm) Ar base flow as carrier gas, and 30 min were required for saturation of the anolyte reservoir with the produced gasses, as visible in Fig. S13. Owing to the strong CO_2 absorption capacity of the alkaline anolyte, with up to 22 g CO_2 absorbed by 1 L of 1 M KOH via formation of carbonate, detection of gaseous CO_2 was limited to a maximum of 500 ppm, as opposed to the 30 000 and 25 000 ppm of N_2 and O_2 detected at 400 mA cm^{-2} over the course of 1 h: nonetheless, the curve of the CO_2 signal follows the trend of N_2 indicating it is genuinely originated by the UOR reaction (Fig. S13). The residual O_2 detected at lower current densities is likely due to minor system leaks. In agreement with previous literature findings [27,30], UOR was found to occur in minor part through the desired $N_2 + CO_2$ pathway even at current densities as low as 25 mA cm^{-2}, and mainly through the nitrite + cyanate, NCO^-, pathway: indeed, the faradaic efficiency distribution for the nitrogen products is 30-40% for N_2, 60-65% for NO_2^- and 0.1-1.5% for NO_3^-, evidencing a prevalence of overoxidation. As reported by Tatarchuck et al., [30] this likely stems from a slight prevalence of isolated catalytic sites in the material, leading to monodentate adsorption of urea with consequent C–N cleavage and overoxidation of nitrogen, as opposed to the case of bridged adsorption on two neighboring catalytic sites, which leads instead to the desired path. As widely reported and consistently with DEMS measurements, under increasingly oxidative conditions, at higher current densities, UOR and OER start to occur simultaneously. A significant OER contribution only appeared above 200 mA cm^{-2}, with a significant decrease of the overoxidation products (FE $NO_x^- = 46\%$) at 400 mA cm^{-2} in favor of O_2 production with a faradaic efficiency of 19%.

Finally, we tested the stability under OER and UOR conditions at 0.1 and 0.2 A cm^{-2} (Fig. S14a and b). Although an initial advantage is found under UOR, a significant increase in UOR voltage is observed over time (20-30 mV h^{-1} at 0.1 A cm^{-2}), as opposed to a stable behavior under OER even over 15 h. However, as evidenced by *post-mortem* SEM characterization (Fig. S15), UOR resulted in a significantly lower damage with respect to OER, with a homogenous residual catalyst coating in the former case. The effects of urea consumption and pH variation induced by carbonate dissolution were excluded as possible causes of UOR activity degradation, since the rate of urea consumption at 0.1 and 0.2 A cm^{-2} is ca. 0.2 and 0.4 g h^{-1}, respectively (with 1 L reservoir, i.e. 20 g urea, meaning 53 h at 0.1 A cm^{-2} for 50% conversion), and the maximum pH variation expected for 100% urea conversion is only 0.5 pH units.

Therefore, we investigated the following possible deterioration mechanisms: a) inactivation of the anodic catalyst by intermediate species or carbon byproducts [73]; b) the decrease in ionic conductivity of the membrane, caused by OH^- exchange with HCO_3^-/CO_3^{2-} anions, in particular considering its possible enhancement due to CO_2 evolution in the confined space of the anodic compartment.

To simulate CO_2 formation during UOR, we bubbled CO_2 at 3 sccm corresponding to theoretical oxidation of urea to N_2 and CO_2 at 0.1 A cm^{-2}, into the 1 M KOH reservoir during OER. This only caused a 7 mV-potential increase over 1 h compared to the pristine OER potential (Fig. 3d), accounting for about 25% of the total degradation observed in UOR. This indicates that performance loss with urea mainly arises from the formation of carbon intermediates, CO* or CNO^- species on the electrode, rather than simple CO_2 adsorption. Indeed, as previously evidenced by DEMS, $Ni(OH)_2$ is likely affected by a slow CO_2 release, which could explain the gradual loss of activity over time.

To further investigate this hypothesis, a chronopotentiostatic measurement at 1.6 V was performed (Fig. S16). The fixed potential was chosen to mainly generate N_2, as confirmed by in-situ GC, and therefore does not reach the level required to produce O_2. This observation is consistent with DEMS data, which clearly indicate a potential window where this condition applies (Fig. 2c). Unlike chronoamperometric measurements, which can trigger a switch from UOR to OER due to the higher potential needed to sustain the selected currents, the chronopotentiostatic method avoids this issue, allowing us to selectively probe UOR. Under these conditions, we observed a clear drop in current overtime; however, after operating in 1 M KOH alone for 2 h and subsequently switching back to KOH with urea, the initial current was almost completely recovered. This indicates a practical strategy to restore catalytic performance by removing detrimental adsorbed carbon intermediates through electrolyte switching.

Furthermore, to simulate the effect of CO_2 production in the confined space of the anode, we conducted additional OER tests in CO_2-saturated 1 M KOH, thus obtaining a carbonate rich anolyte, which resulted in an 80 mV-potential deterioration after 2 h (Fig. S17). The performance decrease in this case is attributed to the loss of ionic conductivity in the membrane: however, since this represents an extreme condition, effectively assessing the extent to which this phenomenon contributes to the performance loss observed during UOR poses a significant challenge.

Ultimately, a more practical way to mitigate electrode degradation is shown in Fig. 4d, which depicts the polarity switching method, performed at 1-h intervals by alternating the current four times between −2 mA cm^{-2} and 10 mA cm^{-2} every 2 min. This methodology proved to be effective in partially restoring the initial potential and limiting the overall potential increase during prolonged operation [10,74].

2.4. Environmental impact and LCA findings

In baseline scenario (primary nickel, no urea addition), the production of 1 kg H_2 resulted associated with the emission of 0.51 kg CO_2-eq, as reported in Table 1. The addition of urea lowered the emission to 0.40-0.48 kg CO_2-eq (respectively, for fresh electrode and for restart

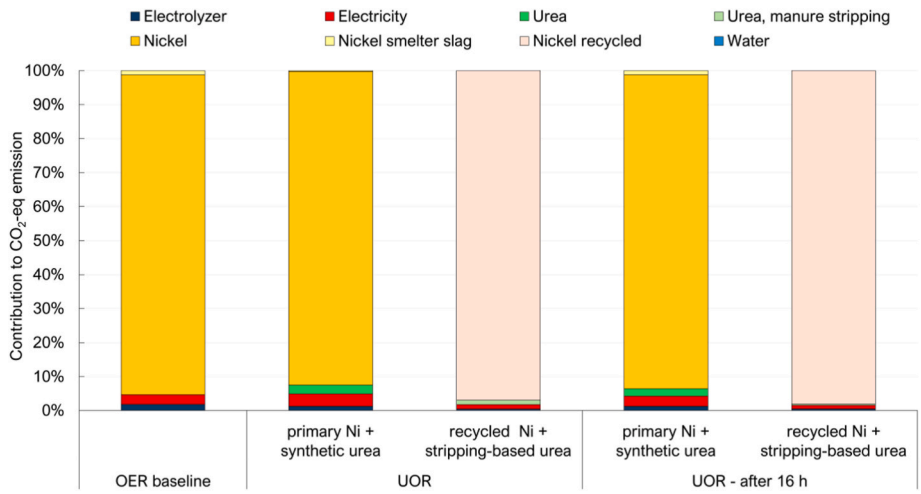

Fig. 4. Impact on CO_2 emission of different factors involved in WE, urea assisted-WE with primary Ni + synthetic urea or urea assisted-WE with circular nickel + urea derived from ammonia-stripping, considering both operation with fresh electrode (UOR) and restart with fresh urea electrolyte after 16 h operation (UOR – after 16 h).

after 16 h of operation, Fig. S16), whereas the use of recycled nickel (with emission factor results obtained from literature) plus stripping-derived urea increased the emission up to 1.13-1.34 kg CO_2-eq. To evaluate the LCA, the term recycled nickel refers form the base material and its origin and not specifically to circular nickel used in this work (see Table 2).

The major contribution to all the scenarios was due to the production and use of nickel, both when it derived from extraction (primary) or from recycling (Fig. 4). The differences in the alternative scenarios can be explained by two different factors: 1) higher efficiency in H_2 production with the use of the same amount of electricity in the scenario with urea addition versus the baseline scenario, 2) the higher impact factor associated with recycled nickel and stripping-based urea versus their original versions (primary and synthetic, respectively).

When considering preliminary results from primary data-based LCA assessment of the circular nickel, an increase in the greenhouse gas emissions could be observed (sens_1), as the obtained factor per unit of nickel is quite higher than that obtained from literature. However, when the system boundaries are expanded to account for the fact that the circular nickel in the analysed system is associated with wastewater treatment, yielding purified water as a co-product and thereby eliminating the need for a separate wastewater treatment process, the results are reversed. In this case, the use of circular nickel leads to a net avoidance of greenhouse gas emissions compared to the OER baseline. The higher negative result obtained for the "UOR - restart after 16 h" scenario was due to the mathematical effect of dividing a negative number by a lower denominator.

Considering all these points, the use of urea could be environmentally positive, as electricity is associated with a not negligible greenhouse gas emission, in particular now that a substantial part is still produced by using fossil-based sources and the impact due to urea production is more than offset by the decreased use of electricity for producing the same amount of H_2. On the other hand, the provision of nickel and urea from systems with high levels of circularity, although in perspective interesting, needs to be assessed carefully, to have high confidence in the possibility that the recycling processes have a lower emission profile with respect to the baseline scenarios. On this point, we need to stress that the impact values available for this type of input is still very scarce, so future studies need to assess in a wider way, with LCA-based approaches and considering other impact categories such as eutrophication or depletion of abiotic resources, the recycling of nickel and the provision of urea based on ammonia captured from other anthropic production systems.

Table 1
CO_2-eq emission impact associated with production of 1 kg of H_2 in the electrolyzer (inventory based on 1 h of electrolyzer operation, see Fig. S16 and Table S4).

Scenario	CO_2 emission (Kg CO_2-eq per Kg H_2)
OER baseline	0.59
UOR	
primary Ni + synthetic urea	0.40
recycled Ni + stripping-based urea	1.13
UOR - restart after 16 h	
primary Ni + synthetic urea	0.48
recycled Ni + stripping-based urea	1.34

Table 2
Results of the sensitivity analysis on the CO_2-eq emission impact associated with production of 1 kg of H_2 in the electrolyzer (circular Ni + stripping-based urea; inventory based on 1 h of electrolyzer operation, see Fig. S16 and Table S4). Reference: emission factor results obtained from literature data for circular Ni. Sens_1/2: emission factor associated with the circular nickel from preliminary LCA based on primary data from Circular Materials, without (sens_1) and with (sens_2) the avoided emissions due to wastewater treatment implied in the circular nickel production.

Scenario	Unit	Reference	sens_1	sens_2
UOR	kg CO_2-eq	1.13	2.65	−1.53
UOR - restart after 16 h	kg CO_2-eq	1.34	3.16	−1.85

3. Conclusion

In this study we demonstrated the feasibility of integrating circular Ni catalysts and urea oxidation into AEMWE technology as a dual strategy for sustainable hydrogen production. Circular $Ni(OH)_2$ and NiO electrocatalysts were recovered from ENP wastewater via CFHS and integrated in anodes for urea-assisted AEMWE. These circular Ni catalysts delivered performances comparable to $Ni(OH)_2$ electrodes prepared from primary nickel, achieving up to a 0.25 V reduction in potential relative to OER and operating optimally below 0.4 A cm^{-2} to avoid OER competition, an operating window for UOR also well-identified by in-situ DEMS analysis. Product analysis by inline GC and IC-CD revealed nitrite (≈60%) as the dominant nitrogen product, followed by nitrogen gas (≈40%), while the adsorption of intermediate species on the catalyst has been revealed as main deactivation step during prolonged operation. Importantly, activity losses could be mitigated through simple polarity or electrolyte switching, offering practical

routes to restore catalyst performance. The LCA also confirms the possibility of reducing overall CO_2-equivalent emissions by obtaining purified water as a co-product of circular Ni production, thereby eliminating the need for a separate wastewater treatment process. Under these conditions, the use of circular nickel and urea results in a net avoidance of greenhouse gas emissions.

Beyond electrochemical performance, the integration of waste recovery and pollutant valorisation underscores the potential of this approach to couple clean energy generation with environmental remediation. Future work should focus on catalyst engineering, enhancing performance stability and steering nitrogen pathways toward N_2, thereby reinforcing both the environmental and economic viability of urea-assisted electrolysis.

Electronic Supporting Information

Full experimental details and methods (synthesis of circular catalysts, details of physicochemical and electrochemical characterization, in situ DEMS, anodes preparation and AEMWE operation, products quantification, LCA analysis) and additional data are available in Electronic Supporting Information.

CRediT authorship contribution statement

Giulia Alice Volpato: Writing – review & editing, Writing – original draft, Methodology, Investigation, Formal analysis, Data curation, Conceptualization. **Andrea Baciami:** Investigation, Data curation. **Kalina Georgieva Kjurchieva:** Investigation, Formal analysis. **Marco Berton:** Methodology, Investigation, Formal analysis, Data curation. **Marco Schiavon:** Methodology, Investigation, Formal analysis, Data curation. **Filippo Bano:** Formal analysis, Data curation. **Alessandra Ferrarini:** Writing – review & editing, Formal analysis. **Silvia Galvanin:** Writing – review & editing, Methodology. **Dario Mosconi:** Writing – review & editing, Formal analysis. **Juan Carlos Calderón:** Methodology, Investigation, Formal analysis, Data curation. **Silvia Pettenuzzo:** Methodology, Investigation, Formal analysis, Data curation. **Elena Colusso:** Methodology, Investigation, Formal analysis, Data curation. **Marco Roverso:** Methodology, Investigation, Formal analysis, Data curation. **Sara Bogialli:** Visualization, Supervision, Methodology. **Elena Pastor:** Writing – review & editing, Supervision, Methodology. **Laura Calvillo:** Writing – review & editing, Supervision. **Stefano Agnoli:** Visualization, Supervision, Funding acquisition. **Mattia Cattelan:** Writing – review & editing, Writing – original draft, Validation, Supervision, Software, Resources, Project administration, Methodology, Investigation, Funding acquisition, Formal analysis, Data curation, Conceptualization.

Declaration of competing interest

The authors declare the following financial interests/personal relationships which may be considered as potential competing interests: Alessandra Ferrarini reports a relationship with Hyter S.r.l. that includes: employment. Silvia Galvanin reports a relationship with Pietro Fiorentini that includes: employment. Dario Mosconi reports a relationship with Circular Materials S.r.l. that includes: employment. If there are other authors, they declare that they have no known competing financial interests or personal relationships that could have appeared to influence the work reported in this paper.

Acknowledgements

G.A.V., M.B., M.S., E.C, and M.C. acknowledge the Centro Studi di Economia e Tecnica dell'Energia "Giorgio Levi Cases" for funding the 2023 Junior Project UNiPHy.

The authors acknowledge support from the C^2 Chemical Complexity project (CUP: C93C22009260001) under the Italian Ministry of University and Research (MUR) program "Dipartimenti di Eccellenza 2023–2027."

M.C. and S.A. acknowledge a research contract on Green Topics from Action IV.6 of the PON Research and Innovation 2014–2020 "Education and Research for Recovery—REACT-EU" program, contract 19-G-12549-1, and Mission 2 ″Green Revolution and Ecological Transition," Component 2 ″Renewable Energy, Hydrogen, Grid, and Sustainable Mobility," Investment 3.5 ″Hydrogen Research and Development," financed by the European Union – Next Generation EU through the SIRIUS project (CUP: F19J22001820004).

L.C. and S.A. acknowledge financial support under the National Recovery and Resilience Plan (NRRP), Mission 4, Component 2, Investment 1.1, Call for Tender No. 1409 published on 14.9.2022 by the Italian MUR, funded by the European Union – NextGenerationEU – Project P2022FALAP (CYCLE-E) (CUP: C53D23007740001).

J.C.C and E.P. acknowledge funding from the Spanish Research Agency (AEI) through project PID 2023-1507070B-I00, funded by MCIN/AEI/10.13039/501100011033, and the Cabildo de Tenerife-TALENTUM program.

Authors A.F. is an employee of Hyter S.r.l., S.G. is an employee of Pietro Fiorentini S.p.A., and author D.M. is an employee of the company Circular Materials S.r.l.; all the companies supplied materials related to this research. The research was funded solely by public funding agencies, and the companies had no role in the study design, data collection, analysis, manuscript preparation, or the decision to publish.

Appendix A. Supplementary data

Supplementary data to this article can be found online at https://doi.org/10.1016/j.ijhydene.2026.154696.

References

[1] Wei S, Sacchi R, Tukker A, Suh S, Steubing B. Future environmental impacts of global hydrogen production. Energy Environ Sci 2024;17:2157–72. https://doi.org/10.1039/D3EE03875K.
[2] Yang B, Zhang R, Shao Z, Zhang C. The economic analysis for hydrogen production cost towards electrolyzer technologies: current and future competitiveness. Int J Hydrogen Energy 2023;48:13767–79. https://doi.org/10.1016/j.ijhydene.2022.12.204.
[3] Du N, Roy C, Peach R, Turnbull M, Thiele S, Bock C. Anion-exchange membrane water electrolyzers. Chem Rev 2022;122:11830–95. https://doi.org/10.1021/acs.chemrev.1c00854.
[4] Wang J, Gao Y, Kong H, Kim J, Choi S, Ciucci F, et al. Non-precious-metal catalysts for alkaline water electrolysis: *operando* characterizations, theoretical calculations, and recent advances. Chem Soc Rev 2020;49:9154–96. https://doi.org/10.1039/D0CS00575D.
[5] Shiva Kumar S, Himabindu V. Hydrogen production by PEM water electrolysis – a review. Mater Sci Energy Technol 2019;2:442–54. https://doi.org/10.1016/j.mset.2019.03.002.
[6] Shih AJ, Monteiro MCO, Dattila F, Pavesi D, Philips M, da Silva AHM, et al. Water electrolysis. Nat Rev Methods Primers 2022;2:84. https://doi.org/10.1038/s43586-022-00164-0.
[7] Cattelan M, Yang J, Cielo L, Nappini S, Carlotto S, Nalesso M, et al. Operando exploration of CoAl-LDH: transformations driving alkaline oxygen evolution reaction. Small 2025;21:2412351. https://doi.org/10.1002/smll.202412351.
[8] Hu C, Lee YJ, Ma Y, Zhang X, Jung SW, Hwang H, et al. Advanced patterned membranes for efficient alkaline membrane electrolyzers. ACS Energy Lett 2024;9:1219–27. https://doi.org/10.1021/acsenergylett.4c00207.
[9] Faid AY, Sunde S. Anion exchange membrane water electrolysis from catalyst design to the membrane electrode assembly. Energy Technol 2022;10. https://doi.org/10.1002/ente.202200506.
[10] Sha Q, Wang S, Yan L, Feng Y, Zhang Z, Li S, et al. 10,000-h-stable intermittent alkaline seawater electrolysis. Nature 2025;639:360–7. https://doi.org/10.1038/s41586-025-08610-1.
[11] Yang Y, Li P, Zheng X, Sun W, Dou SX, Ma T, et al. Anion-exchange membrane water electrolyzers and fuel cells. Chem Soc Rev 2022;51:9620–93. https://doi.org/10.1039/D2CS00038E.
[12] Wu J, Xia Q, Li Z. Green innovation and enterprise green total factor productivity at a micro level: a perspective of technical distance. J Clean Prod 2022;344:131070. https://doi.org/10.1016/j.jclepro.2022.131070.
[13] Iea. Technology Roadmap Energy. GHG reductions in the chemical industry via catalytic processes. 2013.
[14] Energy Agency I. Ammonia technology roadmap towards more sustainable nitrogen fertiliser production. n.d.
[15] energy agency international. CO2 emissions in 2022. 2022.

[16] Urbańczyk E, Sowa M, Simka W. Urea removal from aqueous solutions—a review. J Appl Electrochem 2016;46:1011–29. https://doi.org/10.1007/s10800-016-0993-6.

[17] Ravi R, Beyers M, Vingerhoets R, Brienza C, Luo H, Bruun S, et al. In the quest for sustainable management of liquid fraction of manure - insights from a life cycle assessment. Sustain Prod Consum 2023;43:251–63. https://doi.org/10.1016/j.spc.2023.11.006.

[18] Gao X, Zhang S, Wang P, Jaroniec M, Zheng Y, Qiao S-Z. Urea catalytic oxidation for energy and environmental applications. Chem Soc Rev 2024;53:1552–91. https://doi.org/10.1039/D3CS00963G.

[19] Cao Z, Zhou T, Ma X, Shen Y, Deng Q, Zhang W, et al. Hydrogen production from urea sewage on NiFe-Based porous electrocatalysts. ACS Sustainable Chem Eng 2020. https://doi.org/10.1021/acssuschemeng.0c04049. acssuschemeng.0c04049.

[20] Liu D, Liu T, Zhang L, Qu F, Du G, Asiri AM, et al. High-performance urea electrolysis towards less energy-intensive electrochemical hydrogen production using a bifunctional catalyst electrode. J Mater Chem A Mater 2017;5:3208–13. https://doi.org/10.1039/C6TA11127K.

[21] Yang C, Pang H, Li X, Zheng X, Wei T, Ma X, et al. Scalable electrocatalytic urea wastewater treatment coupled with hydrogen production by regulating adsorption behavior of urea molecule. Nano-Micro Lett 2025;17:159. https://doi.org/10.1007/s40820-024-01585-0.

[22] Xiao Z, Qian Y, Tan T, Lu H, Liu C, Wang B, et al. Energy-saving hydrogen production by water splitting coupling urea decomposition and oxidation reactions. J Mater Chem A Mater 2023;11:259–67. https://doi.org/10.1039/D2TA07152E.

[23] Cattelan M, Calvillo L, Agnoli S. Improved mass transport imparts stability and durability in nickel catalysts for urea oxidation. Chem Catal 2022;2:2835–6. https://doi.org/10.1016/j.checat.2022.10.024.

[24] Kim S, Piao G, Han DS, Shon HK, Park H. Solar desalination coupled with water remediation and molecular hydrogen production: a novel solar water-energy nexus. Energy Environ Sci 2018;11:344–53. https://doi.org/10.1039/C7EE02640D.

[25] Xu S, Ruan X, Ganesan M, Wu J, Ravi SK, Cui X. Transition metal-based catalysts for urea oxidation reaction (UOR): Catalyst design strategies, applications, and future perspectives. Adv Funct Mater 2024;34. https://doi.org/10.1002/adfm.202313309.

[26] Zhang Y, Lei Y, Yan Y, Cai W, Huang J, Lai Y, et al. Enhancing hydrogen production capability from urine-containing sewage through optimization of urea oxidation pathways. Appl Catal B Environ Energy 2024;353:124064. https://doi.org/10.1016/j.apcatb.2024.124064.

[27] Gao X, Bai X, Wang P, Jiao Y, Davey K, Zheng Y, et al. Boosting urea electrooxidation on oxyanion-engineered nickel sites via inhibited water oxidation. Nat Commun 2023;14:5842. https://doi.org/10.1038/s41467-023-41588-w.

[28] Wang D, Yan W, Vijapur SH, Botte GG. Enhanced electrocatalytic oxidation of urea based on nickel hydroxide nanoribbons. J Power Sources 2012;217:498–502. https://doi.org/10.1016/j.jpowsour.2012.06.029.

[29] Zemtsova VM, Oshchepkov AG, Savinova ER. Unveiling the role of iron in the nickel-catalyzed urea oxidation reaction. ACS Catal 2023;13:13466–73. https://doi.org/10.1021/acscatal.3c03126.

[30] Tatarchuk SW, Medvedev JJ, Li F, Tobolovskaya Y, Klinkova A. Nickel-catalyzed urea electrolysis: from nitrite and cyanate as major products to nitrogen evolution. Angew Chem Int Ed 2022;61. https://doi.org/10.1002/anie.202209839.

[31] Haghverdi Khamene S, van Helvoirt C, Tsampas MN, Creatore M. Electrochemical activation of atomic-layer-deposited nickel oxide for water oxidation. J Phys Chem C 2023;127:22570–82. https://doi.org/10.1021/acs.jpcc.3c05002.

[32] Gong M, Wang D-Y, Chen C-C, Hwang B-J, Dai H. A mini review on nickel-based electrocatalysts for alkaline hydrogen evolution reaction. Nano Res 2016;9:28–46. https://doi.org/10.1007/s12274-015-0965-x.

[33] Vij V, Sultan S, Harzandi AM, Meena A, Tiwari JN, Lee W-G, et al. Nickel-based electrocatalysts for energy-related applications: oxygen reduction, oxygen evolution, and hydrogen evolution reactions. ACS Catal 2017;7:7196–225. https://doi.org/10.1021/acscatal.7b01800.

[34] Lupi C, Dell'Era A, Pasquali M. Nickel–cobalt electrodeposited alloys for hydrogen evolution in alkaline media. Int J Hydrogen Energy 2009;34:2101–6. https://doi.org/10.1016/j.ijhydene.2009.01.015.

[35] Xu X, Yu X, Guo K, Dong L, Miao X. Alkaline media regulated NiFe-LDH-Based nickel–iron phosphides toward robust overall water splitting. Catalysts 2023;13:198. https://doi.org/10.3390/catal13010198.

[36] Jiang J, Zhang A, Li L, Ai L. Nickel–cobalt layered double hydroxide nanosheets as high-performance electrocatalyst for oxygen evolution reaction. J Power Sources 2015;278:445–51. https://doi.org/10.1016/j.jpowsour.2014.12.085.

[37] Sun F, Wang G, Ding Y, Wang C, Yuan B, Lin Y. NiFe-Based metal–organic framework nanosheets directly supported on nickel foam acting as robust electrodes for electrochemical oxygen evolution reaction. Adv Energy Mater 2018;8. https://doi.org/10.1002/aenm.201800584.

[38] Wilhelm M, Bastos A, Neves C, Martins R, Tedim J. Ni-Fe layered double hydroxides for oxygen evolution reaction: impact of Ni/Fe ratio and crystallinity. Mater Des 2021;212:110188. https://doi.org/10.1016/j.matdes.2021.110188.

[39] Drevon D, Görlin M, Chernev P, Xi L, Dau H, Lange KM. Uncovering the role of oxygen in Ni-Fe(OxHy) electrocatalysts using in situ soft X-ray absorption spectroscopy during the oxygen evolution reaction. Sci Rep 2019;9:1532. https://doi.org/10.1038/s41598-018-37307-x.

[40] Tang P, Di Vizio B, Yang J, Patil B, Cattelan M, Agnoli S. Fe,Ni-Based metal–organic frameworks embedded in nanoporous nitrogen-doped graphene as a highly efficient electrocatalyst for the oxygen evolution reaction. Nanomaterials 2024;14:751. https://doi.org/10.3390/nano14090751.

[41] Salvò D, Mosconi D, Neyman A, Bar-Sadan M, Calvillo L, Granozzi G, et al. Nanoneedles of mixed transition metal phosphides as bifunctional catalysts for electrocatalytic water splitting in alkaline media. Nanomaterials 2023;13:683. https://doi.org/10.3390/nano13040683.

[42] Cai M, Zhu Q, Wang X, Shao Z, Yao L, Zeng H, et al. Formation and stabilization of NiOOH by introducing α-FeOOH in LDH: composite electrocatalyst for oxygen evolution and urea oxidation reactions. Adv Mater 2023;35. https://doi.org/10.1002/adma.202209338.

[43] Veettil VT, Vijayakumar AU, Ashdot A, Zitoun D. Precious-group-metal-free energy-efficient urea electrolysis: membrane electrode assembly cell using Ni_3N nanoparticles as catalyst. ACS Appl Energy Mater 2022;5:1397–402. https://doi.org/10.1021/acsaem.1c03689.

[44] Bersani M. Method for treating wastewater for the recovery of metals contained therein, and apparatus for SUCH a method. WO2021089403A1. 2021.

[45] Darr JA, Zhang J, Makwana NM, Weng X. Continuous hydrothermal synthesis of inorganic nanoparticles: applications and future directions. Chem Rev 2017;117:11125–238. https://doi.org/10.1021/acs.chemrev.6b00417.

[46] Mosconi D, Blanco M, Ran J, Sturaro M, Bersani M, Granozzi G. Selective and scaled-up continuous flow synthesis of manganese oxide nanocatalysts for single electron transfer reactions. Chem Eng J 2021;417:129063. https://doi.org/10.1016/j.cej.2021.129063.

[47] Loto CA. Electroless nickel plating – a review. Silicon 2016;8:177–86. https://doi.org/10.1007/s12633-015-9367-7.

[48] Meyer JS, Santore RC, Bobbitt JP, DeBrey LD, Boese CJ, Paquin PR, et al. Binding of nickel and copper to fish gills predicts toxicity when water hardness varies, but free-ion activity does not. Environ Sci Technol 1999;33:913–6. https://doi.org/10.1021/es980715q.

[49] Denkhaus E, Salnikow K. Nickel essentiality, toxicity, and carcinogenicity. Crit Rev Oncol Hematol 2002;42:35–56. https://doi.org/10.1016/S1040-8428(01)00214-1.

[50] Chen C, Huang D, Liu J. Functions and toxicity of nickel in plants: recent advances and future prospects. Clean 2009;37:304–13. https://doi.org/10.1002/clen.200800199.

[51] Baldassarre B, Carrara S. Critical raw materials, circular economy, sustainable development: EU policy reflections for future research and innovation. Resour Conserv Recycl 2025;215:108060. https://doi.org/10.1016/j.resconrec.2024.108060.

[52] Gnedovets AG, Ankudinov AB, Zelenskii VA, Alymov MI. Creation of highly porous material with a hierarchical structure by sintering of nickel nanopowder using ammonium bicarbonate as space holder. Inorg Mater: Applied Research 2019;10:451–8. https://doi.org/10.1134/S2075113319020126.

[53] Mahala C, Devi Sharma M, Basu M. Fe-doped nickel hydroxide/nickel oxyhydroxide function as an efficient catalyst for the oxygen evolution reaction. Chemelectrochem 2019;6:3488–98. https://doi.org/10.1002/celc.201900857.

[54] Wu X, Gong K, Zhao G, Lou W, Wang X, Liu W. Mechanical synthesis of chemically bonded phosphorus–graphene hybrid as high-temperature lubricating oil additive. RSC Adv 2018;8:4595–603. https://doi.org/10.1039/C7RA11691H.

[55] Hall DS, Lockwood DJ, Bock C, MacDougall BR. Nickel hydroxides and related materials: a review of their structures, synthesis and properties. Proc R Soc A 2015;471:20140792. https://doi.org/10.1098/rspa.2014.0792.

[56] Hall DS, Lockwood DJ, Poirier S, Bock C, MacDougall BR. Raman and infrared spectroscopy of α and β phases of thin nickel hydroxide films electrochemically formed on nickel. J Phys Chem A 2012;116:6771–84. https://doi.org/10.1021/jp303546r.

[57] Hall DS, Lockwood DJ, Poirier S, Bock C, MacDougall BR. Applications of in situ raman spectroscopy for identifying nickel hydroxide materials and surface layers during chemical aging. ACS Appl Mater Interfaces 2014;6:3141–9. https://doi.org/10.1021/am405419k.

[58] Bantignies JL, Deabate S, Righi A, Rols S, Hermet P, Sauvajol JL, et al. New insight into the vibrational behavior of nickel hydroxide and oxyhydroxide using inelastic neutron scattering, Far/mid-infrared and raman spectroscopies. J Phys Chem C 2008;112:2193–201. https://doi.org/10.1021/jp075819e.

[59] Mironova-Ulmane N, Kuzmin A, Sildos I, Puust L, Grabis J. Magnon and phonon excitations in nanosized NiO. Latv J Phys Tech Sci 2019;56:61–72. https://doi.org/10.2478/lpts-2019-0014.

[60] Stern L-A, Hu X. Enhanced oxygen evolution activity by NiO_x and $Ni(OH)_2$ nanoparticles. Faraday Discuss 2014;176:363–79. https://doi.org/10.1039/C4FD00120F.

[61] Trotochaud L, Young SL, Ranney JK, Boettcher SW. Nickel–iron oxyhydroxide oxygen-evolution electrocatalysts: the role of intentional and incidental iron incorporation. J Am Chem Soc 2014;136:6744–53. https://doi.org/10.1021/ja502379c.

[62] Wang Y, Qian G, Xie Z, Yu H, Li L, Li J, et al. Strengthening CuNiCoMo medium-entropy alloy by tuning local lattice tensile strain and built-in electric field for boosting urea oxidation reaction. Appl Catal B Environ Energy 2025;365:124841. https://doi.org/10.1016/j.apcatb.2024.124841.

[63] Li L, Ge L, Qian G, Wang Y, Li J, Cao X, et al. Interfacial lattice strain and electronic transfer induced by lignin-derived carbon coupled with Ni-Mn2Mo3O8 heterojunction for improving industrial-level urea electrolysis. Appl Catal B Environ Energy 2025;377:125465. https://doi.org/10.1016/j.apcatb.2025.125465.

[64] Cao X, Li L, Qian G, Xie Q, Xie Y, Li J, et al. Optimization of interfacial electrons and compressive-tensile strains at lignin-derived carbon-supported multiphase Ni/Cu/MoO_2 interfaces for boosting large current-density HER. Small 2025;21. https://doi.org/10.1002/smll.202501176.

[65] Li L, Qian G, Ge L, Wang Y, Cao X, Li J, et al. Embedding Mn2Mo3O8/Ni heterojunctions in self-supported lignin-derived carbon frameworks for enhanced ampere-level hydrogen evolution reaction under pH-universal conditions. Chem Eng J 2025;522:166556. https://doi.org/10.1016/j.cej.2025.166556.
[66] Cao X, Xie Q, Xie Y, Li J, Li L, Xu Y, et al. Synergistic multiphase lattice strains and built-in electric field in lignin-derived carbon coupled with Mo-Cu-Ni multimetallic for enhanced urea-assisted water electrolysis. Chem Eng J 2025;521:166557. https://doi.org/10.1016/j.cej.2025.166557.
[67] Li J, Wang Y, Chen C, Cao X, Li L, Xu Y, et al. A high-efficiency urea electrolysis catalyst: sulfur-doped lignin-derived carbon-encapsulated NiCo@MoO2 with triphasic interface and superhydrophilic/superaerophobic surfaces. Chem Eng J 2025;522:167733. https://doi.org/10.1016/j.cej.2025.167733.
[68] Li L, Xu H, Qian G, Cao X, Li J, Xu Y, et al. MoO $_2$ -mediated Ni—Fe bond contraction and electronic modulation in Ni $_3$ Fe alloy for efficient water electrolysis at high-current-densities. Adv Mater 2026;38. https://doi.org/10.1002/adma.202512658.
[69] Li J, Li J, Liu T, Chen L, Li Y, Wang H, et al. Deciphering and suppressing over-oxidized nitrogen in nickel-catalyzed urea electrolysis. Angew Chem Int Ed 2021; 60:26656–62. https://doi.org/10.1002/anie.202107886.
[70] Zhan G, Hu L, Li H, Dai J, Zhao L, Zheng Q, et al. Highly selective urea electrooxidation coupled with efficient hydrogen evolution. Nat Commun 2024;15: 5918. https://doi.org/10.1038/s41467-024-50343-8.
[71] Vedharathinam V, Botte GG. Understanding the electro-catalytic oxidation mechanism of urea on nickel electrodes in alkaline medium. Electrochim Acta 2012;81:292–300. https://doi.org/10.1016/j.electacta.2012.07.007.
[72] Bano F, Chen D, Perilli D, Zambonin S, Mosconi D, Roverso M, et al. Enhanced urea oxidation reaction by Mn-doped nickel hydroxide from wastewater. 2026. submitted for publication.
[73] Ma Y, Ma C, Wang Y, Wang K. Advanced nickel-based catalysts for urea oxidation reaction: challenges and developments. Catalysts 2022;12:337. https://doi.org/10.3390/catal12030337.
[74] Han S, Kim S, Cho HJ, Lee JY, Ryu J, Yoon J. Dynamic polarization control of Ni electrodes for sustainable and scalable water electrolysis under alkaline conditions. Nat Commun 2025;16:4803. https://doi.org/10.1038/s41467-025-60201-w.